

Article

Combining Computational Modelling and Machine Learning to Identify COVID-19 Patients with a High Thromboembolism Risk

Anass Bouchnita ^{1,*}, Anastasia Mozokhina ² , Patrice Nony ^{3,4}, Jean-Pierre Llored ⁵ and Vitaly Volpert ^{2,6}¹ Department of Mathematical Sciences, The University of Texas at El Paso, El Paso, TX 79968, USA² People's Friendship University of Russia (RUDN), Moscow 117198, Russia³ Service de Pharmacologie Clinique, Hospices Civils de Lyon, 69002 Lyon, France⁴ UMR CNRS 5558, University Claude Bernard Lyon 1, 69100 Lyon, France⁵ Ecole Centrale Casablanca, Casablanca 20000, Morocco⁶ Institut Camille Jordan, UMR 5208 CNRS, University Claude Bernard Lyon 1, 69622 Villeurbanne, France

* Correspondence: abouchnita@utep.edu

Abstract: Severe acute respiratory syndrome of coronavirus 2 (SARS-CoV-2) is a respiratory virus that disrupts the functioning of several organ systems. The cardiovascular system represents one of the systems targeted by the novel coronavirus disease (COVID-19). Indeed, a hypercoagulable state was observed in some critically ill COVID-19 patients. The timely prediction of thrombosis risk in COVID-19 patients would help prevent the incidence of thromboembolic events and reduce the disease burden. This work proposes a methodology that identifies COVID-19 patients with a high thromboembolism risk using computational modelling and machine learning. We begin by studying the dynamics of thrombus formation in COVID-19 patients by using a mathematical model fitted to the experimental findings of in vivo clot growth. We use numerical simulations to quantify the upregulation in the size of the formed thrombi in COVID-19 patients. Next, we show that COVID-19 upregulates the peak concentration of thrombin generation (TG) and its endogenous thrombin potential. Finally, we use a simplified 1D version of the clot growth model to generate a dataset containing the hemostatic responses of virtual COVID-19 patients and healthy subjects. We use this dataset to train machine learning algorithms that can be readily deployed to predict the risk of thrombosis in COVID-19 patients.

Keywords: blood coagulation; thrombosis; Navier–Stokes equations; computational fluid dynamics; neural networks

MSC: 92B05; 76Z05



Citation: Bouchnita, A.; Mozokhina, A.; Nony, P.; Llored, J.-P.; Volpert, V. Combining Computational Modelling and Machine Learning to Identify COVID-19 Patients with a High Thromboembolism Risk. *Mathematics* **2023**, *11*, 289. <https://doi.org/10.3390/math11020289>

Academic Editor: Ioannis G. Stratis

Received: 17 October 2022

Revised: 9 November 2022

Accepted: 15 November 2022

Published: 5 January 2023



Copyright: © 2023 by the authors. Licensee MDPI, Basel, Switzerland. This article is an open access article distributed under the terms and conditions of the Creative Commons Attribution (CC BY) license (<https://creativecommons.org/licenses/by/4.0/>).

1. Introduction

The coronavirus disease (COVID-19) emerged in Wuhan, China in late 2019 and represents a major threat to global health, as it is caused by a highly transmissible virus. The severe forms of COVID-19 may lead to death by causing pneumonia. However, critically ill patients also experience a hypercoagulable state, which increases the risk and incidence of thromboembolic events. Indeed, it was reported that 20% to 50% of COVID-19 patients experience changes in their coagulation profile [1]. These changes include an elevated D-dimer, platelet count, and fibrinogen, in addition to a lower thromboplastin time. These changes are associated with a higher incidence of bleeding and thrombosis in COVID-19 patients. Indeed, 25% of patients in intensive-care units (ICU) develop venous thromboembolism, and 8% die from it [2].

The pathogenesis of thrombosis in COVID-19 patients is not completely understood. However, several mechanisms explaining the association between thrombosis and COVID-19 have recently been identified [3]. First, COVID-19 increases the risk of endothelial injuries

and dysfunction. Severe acute respiratory syndrome of coronavirus 2 (SARS-CoV-2) targets endothelial cells, which leads to their apoptosis by cytotoxicity [4]. Second, SARS-CoV-2 infection induces a cytokine storm that provokes an immuno-thrombo-inflammation, similar to the one observed in acute respiratory disease syndrome (ARDS) [5]. A third identified mechanism concerns the activation of platelets by SARS-CoV-2 antibodies [6]. Platelets derived from COVID-19 patients show a higher expression of Ca^{2+} and phospholipid (PS) externalization in comparison with healthy subjects. Finally, an *in vivo* study demonstrated that COVID-19 autoantibodies upregulate the generation of thrombin during clotting by acting on the coagulation cascade. These autoantibodies upregulate neutrophils activity, including the release of neutrophil extracellular trap (NET) [7]. This protein enhances thrombin generation (TG) through the intrinsic pathway of the coagulation cascade, which increases the risk of both blood clot formation and vascular occlusion [8].

Blood coagulation is a physiological process that has already been studied using a wide variety of mathematical modelling techniques. Patient-specific kinetics of thrombin generation were explored using systems of ordinary differential equations [9,10]. The spatio-temporal dynamics of thrombus formation in the flow can be described by coupling advection–reaction–diffusion equations for clotting factors with the Navier–Stokes equations for blood flow [11–16]. Multiphase models were also used to describe the process of thrombus formation in complex geometries such as aneurysms and recirculation areas [17–19]. Discrete methods, such as dissipative particle dynamics and the immersed boundary method, were also applied to accurately capture the interplay between blood flow and blood cells [20,21]. Finally, multiscale models aim to combine discrete and continuous modelling techniques to describe thrombus formation [22,23]. These methods are especially useful in modelling arterial thrombi because it is a process that is mainly regulated by platelet interactions. Recently, some of these modeling techniques were applied to study thrombosis development in COVID-19. A fine-grained DPD model was used to investigate the role of platelets, white blood cells, and coagulation factors in the parthenogenesis of thrombosis in COVID-19 [24]. The modeling has revealed that factor V and antithrombin are the most important coagulation factors that influence thrombus formation. They also showed that the recruitment of white blood cells to the endothelium exacerbates blood clotting. Another model focused on the kinetics of thrombin generation in COVID-19 patients [25]. The model has shown that the lack of antithrombin and the excess of fibrinogen significantly influence the risk of thrombosis. In a previous study, we used a multiscale model to quantify the effect of vessel obstruction on blood circulation as a result of lung inflammation in COVID-19 [26]. We showed that an obstruction level of 5% leads to a decrease in blood flux by 12%.

Machine learning is a technique that can be used for the diagnosis of disease such as thrombosis [27,28]. The advantage of machine learning algorithms is that they can offer timely and accurate predictions. However, their training requires access to a massive amount of data, and it is not possible to interpret their predictions. Recently, we have developed a novel methodology that combines mathematical modeling and deep learning to predict the response of patients to anticoagulant therapy in a fast and explainable manner [29]. This new approach used computational-fluid dynamics simulations to predict the coagulation response of patients receiving anticoagulant drugs. The obtained results were used as a dataset to train a neural network architecture that quickly predicts the patient-specific response. The predictions of the neural networks are then explained using systematic numerical simulations of the underlying computational model. In this work, we propose to use the same methodology to evaluate the risk of thrombosis in COVID-19 patients. We begin by modelling thrombus formation in COVID-19 patients using a previously developed model and available experimental data. Next, we characterize the generation of thrombin in COVID-19 patients. Finally, we use a 1D version of the model to generate a large dataset of hemostatic responses in COVID-19 patients and healthy subjects. This dataset is used to train a machine learning algorithm that can be readily applied to predict the risk of thrombosis in COVID-19 patients.

2. Mathematical Modelling of Thrombus Formation and Thrombin Generation in COVID-19

In this section, we introduce a mathematical model that can be used to simulate venous thrombus formation in the flow. The model describes thrombin generation as observed in real patients. It can be extended to simulate the spatio-temporal dynamics of clot growth. We describe how this model can be applied to model COVID-19-associated thrombosis.

2.1. Thrombin Generation Modelling

We use a previously developed model to describe thrombin generation [30]:

$$\frac{\partial[Va]}{\partial t} = k_1T - h_1[Va], \tag{1}$$

$$\frac{\partial[VIIIa]}{\partial t} = k_2T - h_2[VIIIa], \tag{2}$$

$$\frac{\partial[XIa]}{\partial t} = k_3T - h_3[XIa], \tag{3}$$

$$\frac{\partial[IXa]}{\partial t} = k_4[XIa] - h_4[IXa], \tag{4}$$

$$\frac{\partial U}{\partial t} = (\bar{k}_5[TF] + k_5[XIa] + k_{55}[VIIIa][IXa])(U^0 - U) - h_5U, \tag{5}$$

$$\frac{\partial T}{\partial t} = (k_6U + k_{66}U[Va])P - K_9T, \tag{6}$$

where k_i denotes the activation coefficient rates and h_i the inhibition rates. The factors Va and Xa form the prothrombinase complex $Va - Xa$, and $VIIIa$ and IXa constitute the complex $VIIIa - IXa$. They are introduced in (5) and (6) in the form of the terms $k_{55}[VIIIa][IXa]$ and $k_{66}U[Va]$, obtained using the assumption of detailed equilibrium for fast reactions. The concentrations of coagulation factors can be expressed as follows:

$$[Va] = \frac{k_1}{h_1}T, \quad [VIIIa] = \frac{k_2}{h_2}T, \quad [XIa] = \frac{k_3}{h_3}T, \quad [IXa] = \frac{k_3k_4}{h_3h_4}T, \tag{7}$$

and assuming that Equation (5) has reached equilibrium during the amplification phase ($\bar{k}_5[TF] = 0$ and consider a zero-order reaction instead of a first-order one), we obtain, using the detailed equilibrium assumption:

$$[Xa] = \frac{k_3k_4}{h_3h_4}T \left(\frac{k_5}{h_5} + \frac{k_5k_2}{h_2h_5} \right). \tag{8}$$

Substituting these concentrations with their expression in (5) and (6), we obtain two equations for factor XI (U) and thrombin (T), and we add to the system one equation for prothrombin (P):

$$\frac{\partial U}{\partial t} = (K_1 + K_2T + K_3T^2)(U^0 - U) - K_4U, \tag{9}$$

$$\frac{\partial P}{\partial t} = -(K_5U + K_6T + K_7T^2 + K_8T^3)P, \tag{10}$$

$$\frac{\partial T}{\partial t} = (K_5U + K_6T + K_7T^2 + K_8T^3)P - K_9T, \tag{11}$$

where

$$K_1 = \bar{k}_5[TF], \quad K_2 = \frac{k_5k_4k_3}{h_4h_3}, \quad K_3 = \frac{k_{55}k_2k_4k_3}{h_2h_4h_3}, \quad K_4 = h_5, \tag{12}$$

$$K_5 = k_6, \quad K_6 = \frac{k_3k_4k_5k_6}{h_3h_4h_5}, \quad K_7 = \frac{k_2k_3k_4k_5k_6}{h_2h_3h_4h_5} + \frac{k_1k_3k_4k_5k_6}{h_1h_3h_4h_5}, \quad K_8 = \frac{k_1k_2k_3k_4k_5k_6}{h_1h_2h_3h_4h_5}.$$

These expressions are obtained by applying the detailed equilibrium approximation for fast reactions on the system (1)–(6). The reduced model gives a good approximation of the rate of clot growth described by the system (1)–(6) [10]. The nine parameters K_1, K_2, \dots, K_9 can be fitted to approximate the thrombin generation curves of real patients [10]. In this work, we fit the model to thrombin generation curves of a patient with a normal coagulation response. Then, we introduce the effect of COVID-19 autoantibodies on the thrombin generation kinetics to simulate the hypercoagulable state associated with COVID-19.

2.2. Clot Formation in the Flow

2.2.1. Spatio-Temporal Distribution of Clotting Factors

We incorporate diffusion and transport by flow in the previously introduced model of thrombin generation [11]. We describe the spatial distributions of factor XIa (U), thrombin (T), and prothrombin (P) as follows:

$$\frac{\partial U}{\partial t} + \nabla \cdot (\mathbf{u}U - D_t \nabla U) = (K_2T + K_3T^2)(U^0 - U) - K_4U, \tag{13}$$

$$\frac{\partial T}{\partial t} + \nabla \cdot (\mathbf{u}T - D_t \nabla T) = (K_5U + \frac{K_6T + K_7T^2 + K_8T^3}{1 + \sigma C})P - K_9T, \tag{14}$$

$$\frac{\partial P}{\partial t} + \nabla \cdot (\mathbf{u}P - D_t \nabla P) = -(K_5U + \frac{K_6T + K_7T^2 + K_8T^3}{1 + \sigma C})P. \tag{15}$$

Here, the second terms in the left-hand side of the three equations describe the diffusion of these three proteins and their transport by blood flow. For prothrombin, we prescribe an initial and left boundary condition of $P = P_0$ and a zero-flux condition at the rest of boundaries. We consider a zero-flux boundary condition for thrombin and factor Xa everywhere, except on the injury site, where we consider the following condition describing the activation of factor X by the complex TF-FVIIa during the initiation stage [12]:

$$\frac{\partial U}{\partial \mathbf{n}} = \frac{K_1(U^0 - U)}{D(1 + \beta_1(U^0 - U))}. \tag{16}$$

Next, we consider the activated protein C (APC), which localizes the formation of the clot by stopping the propagation of thrombin near healthy tissues. APC is activated by the complex thrombin–thrombomodulin and downregulates the production of thrombin by inhibiting the activation of several factors, such as factor V and factor VIII. We describe its distribution as follows:

$$\frac{\partial C}{\partial t} + \nabla \cdot (\mathbf{u}C - D_t \nabla C) = -K_{10}C. \tag{17}$$

We apply the zero-flux boundary condition everywhere for APC except on healthy tissues where protein C is activated by the thrombin-thrombomodulin complex [12]:

$$\frac{\partial C}{\partial \mathbf{n}} = \frac{\alpha_2 T(C^0 - C)}{D(1 + \beta_2(C^0 - C))}. \tag{18}$$

After that, we add the equations for fibrin polymerization:

$$\frac{\partial F_g}{\partial t} + \nabla \cdot (\mathbf{u}F_g - D_f \nabla F_g) = -K_{11}TF_g, \tag{19}$$

$$\frac{\partial F}{\partial t} + \nabla \cdot (\mathbf{u}F - D_f \nabla F) = K_{11}TF_g - K_{12}F, \tag{20}$$

$$\frac{\partial F_p}{\partial t} = K_{12}F. \tag{21}$$

Here, F_g , F , and F_p describe the concentrations of fibrinogen, fibrin, and fibrin polymer, respectively. Fibrin polymer does not diffuse and it is not transported by flow. Therefore, we do not consider a diffusion and advection term in the equation for fibrin polymer. We prescribe the inlet and initial condition of $F_g = F_{g0}$ for fibrinogen. The zero-flux condition is prescribed at the rest of boundaries. The same condition is applied everywhere for fibrin.

2.2.2. Blood Flow and Clot Mechanobiology

We model blood flow as a non-Newtonian incompressible fluid as follows:

$$\begin{aligned} \rho \frac{\partial \mathbf{u}}{\partial t} + \rho(\mathbf{u} \cdot \nabla) \mathbf{u} &= -\nabla p + \nabla \cdot \tau - \frac{\mu}{K_f} \mathbf{u}, \\ \nabla \cdot \mathbf{u} &= 0, \end{aligned} \tag{22}$$

where \mathbf{u} is the flow velocity, p is the pressure, ρ is the density of the blood, μ is the dynamic viscosity, and τ represents the extra-stress tensor, given by the expression:

$$\tau = 2\mu(\dot{\gamma})D,$$

where $\dot{\gamma}$ is the shear rate. We assume a Carreau rheology model for blood flow [31]:

$$\mu(\dot{\gamma}) = \mu_{inf} + (\mu_0 - \mu_{inf}) \left(1 + (\lambda\dot{\gamma})^2\right)^{\frac{n-1}{2}}.$$

The influence of the clot is captured through the third term on the right-hand side of the equation, where K_f is the hydraulic permeability of the clot [32]:

$$\frac{1}{K_f} = \frac{16}{\alpha^2} \tilde{F}_p^3 \left(1 + 56\tilde{F}_p^3\right). \tag{23}$$

Here, $\tilde{F}_p = \min\left(\frac{1000}{1400}, \frac{F_p}{7000}\right)$ is the normalized concentration of fibrin polymer in the clot, considered to be bounded by a value corresponding to the normal permeability of the clot; α is the radius of fibers.

We assume that blood flow is driven by the pressure difference, and we prescribe the pressure p_{in} at the inlet Γ_{in} and the pressure p_{out} at the outlet Γ_{out} . We consider no-slip boundary conditions $\mathbf{u} = \mathbf{0}$ at the other boundaries $\partial\Omega \setminus (\Gamma_{in} \cup \Gamma_{out})$. To set the inlet pressure as dependent on shear rate parameter γ , we use the formula $p_{in} = 4L\gamma\mu/D$, where L is the length of the vessel and D is the diameter of the vessel. The outflow pressure is set to zero, $p_{out} = 0$.

A solver for the model was implemented using the OpenFoam computational fluid dynamics (CFD) library [33]. The geometry, mesh, and post-processing were performed using tools provided by the same library. The CPU time of a numerical simulation is 23 min on a computer with four cores and 8 GB of RAM. The list of parameter values are available in the appendix section of our previous work [11].

2.3. Modelling the Effect of COVID-19 Antibodies on Blood Coagulability

Thrombosis is one of the serious complications of COVID-19. Lung histopathology has shown evidence of fibrin-based occlusion in small vessels during the advanced stages of the disease [34]. Analysis of blood samples of COVID-19 patients revealed a strong activation of neutrophils [8]. This activation is caused by autoantibodies targeting phospholipids and phospholipid-binding proteins developed by COVID-19 patients [7]. Activated neutrophils release neutrophil extracellular traps (NETs), which promote the formation of blood clots in micro-vessels. To achieve this, NETs upregulate thrombin generation by interacting with microparticles (MPs) expelled by neutrophils. The NET-MP complex promotes thrombin

generation via the intrinsic pathway of coagulation [35]. Indeed, it has been shown that the thrombin generation triggered by the NET-MP complex could be inhibited by blocking factor XII.

Hence, we can model the effect of SARS-CoV-2 autoantibodies on TG by considering that the NET-MP complex upregulates the activation of factor XII. Factor FXIIa upregulates the activation of FXI, which can be described by an elevation in the rate constant k_3 in the system (1)–(6). This constant determines the values of the parameters $K_2, K_3, K_6, K_7,$ and K_8 , as previously demonstrated. Indeed, it is possible to factorize k_3 in all these five parameters. We consider a parameter set corresponding to the thrombin generation curve of a real healthy patient [10]. To quantify the elevation in k_3 caused by COVID-19, we rely on experimental results of mice thrombus formation in healthy blood plasma and after the injection of SARS-CoV-2 autoantibodies. In these experiments, a thrombosis mouse model for the inferior vena cava was considered to study the effect of SARS-CoV-2 autoantibodies on clot growth. A copper wire was inserted in mice’s vena cava and used to activate endothelial cells through electrolysis-mediated free radical generation. The injection of IgG fractions isolated from COVID-19 patients significantly increased the length and the weight of the formed thrombi.

2.4. Machine Learning for Fast Identification of Patients with a Hypercoagulable State Due to COVID-19

After studying the effect of COVID-19 autoantibodies on the dynamics of venous clot growth and thrombin generation, we use the obtained results to train a machine learning algorithm capable of predicting the hemostatic response of COVID-19 patients. To achieve this, we use a simplified version of the model described in Section 2.2 to reduce the CPU time of numerical simulations and to generate a large number of data. The model describes clot propagation in the cross-section perpendicular to the injury site:

$$\frac{\partial U}{\partial t} = \frac{\partial^2 U}{\partial y^2} + (K_2 T + K_3 T^2)(U^0 - U) - K_4 U - \omega \gamma U, \tag{24}$$

$$\frac{\partial T}{\partial t} = \frac{\partial^2 T}{\partial y^2} + (K_5 U + K_6 T + K_7 T^2 + K_8 T^3)P - K_9 T - \omega \gamma T, \tag{25}$$

$$\frac{\partial F}{\partial t} = \frac{\partial^2 F}{\partial y^2} + K_{11} T F_g - K_{12} F, \tag{26}$$

where y represents the y -coordinate, and ω describes the rate of coagulation factor removal by the shear stress. We fit this parameter such that the output of the model approximates the thrombin propagation speed measured using the more complete model [12,36]. After the fitting, we obtain a value of $\omega = 1.31 \times 10^{-3}$. The effect of APC is not considered because we track clot growth near the injury site.

We generate a cohort of 3000 virtual patients by changing the most sensitive model parameters in their physiological ranges. These parameters are $K_2, K_6,$ and K_9 . These parameters can be obtained by fitting models (9) and (11). We have previously identified them as the most sensitive model parameters in a previous work, where a complete sensitivity analysis of the model was conducted [10]. Numerical simulations using this model take only 53 s. The output of the model, which is the height of the formed thrombus, is then classified into three categories: bleeding, if clot growth is insufficient and the size of thrombus is less than 2% of the vessel diameter; normal hemostatic response, for a thrombus size between 2 and 20% of the vessel diameter; and thrombosis, if the clot size exceeds 20% of the diameter.

We consider that half of the virtual patients are critically ill with COVID-19. To model the effect of COVID-19 on blood coagulability, we upregulate the value of the parameter k_3 by 46.5%. Therefore, we obtain a labeled dataset consisting of four features, three for the parameters $K_2, K_6,$ and K_9 , and one corresponds to the illness status (zero for a healthy subject or one for a COVID-19 patient).

3. Results

3.1. Clot Growth Dynamics in COVID-19 Patients

We begin by simulating the dynamics of clot growth in a mouse vena cava under normal conditions [7]. We represent the vena cava with a rectangular domain with a diameter equal to 1.25 mm. We consider a damaged area with a length equal to 0.2 mm, and we fit the concentration of tissue factor at the damaged area such that the final thrombus length is equal to the one observed in experiments (≈ 4 mm). We consider that blood flow is driven by pressure difference between the outlet and inlet such that the shear rate is within the physiological range for venous flows ($\dot{\gamma} = 35 \text{ s}^{-1}$). According to the experiments, the injection of autoantibodies isolated from COVID-19 patients into mice increases the length of the observed thrombi to ≈ 8 mm. To model this, we increase rate constant k_3 that describes FXI activation by FXIIa. This rate constant can be factorized in five of the model parameters: K_2, K_3, K_6, K_7, K_8 . We obtain the desired length by multiplying each of these parameters by 1.465, which corresponds to a 46.5% increase in k_3 .

We show the stages of clot growth in normal blood and after the injection of SARS-CoV-2 autoantibodies in Figure 1. In the healthy subject, clot growth partially occludes the vessel, whereas it completely obstructs the vessel and stops blood circulation in the COVID-19 patient. The corresponding distributions of blood flow velocity are shown in Figure 2. The upregulation in the coagulability of blood in the COVID-19 patient increases thrombin generation, leading to the formation of a bigger clot. Due to the non-Newtonian nature of blood, the development of the clot near the injury site leads to the appearance of a recirculation area behind the clot. This accelerates clot growth as horizontal expansion of the thrombus causes the deceleration of flow above the clot [12].

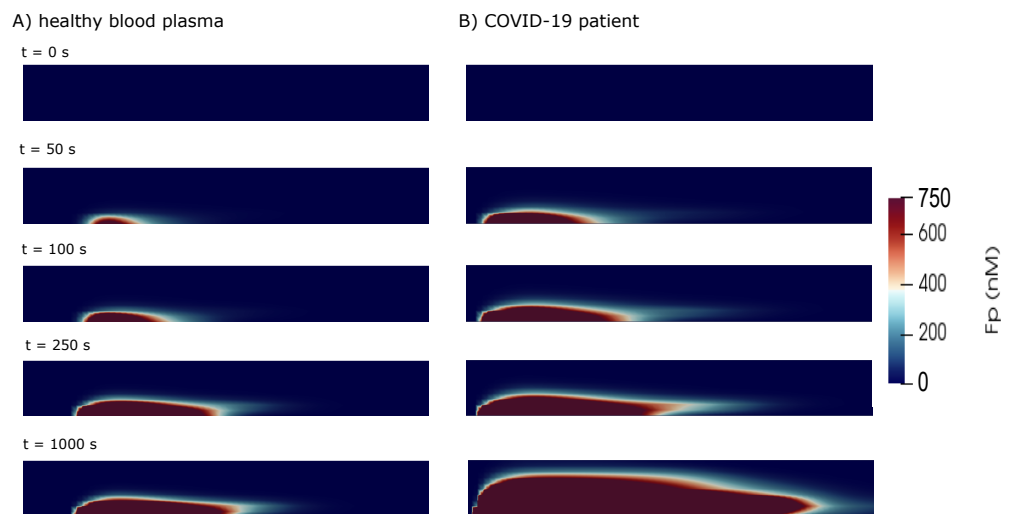


Figure 1. Stages of clot growth for shear rates equal to $\dot{\gamma} = 35 \text{ s}^{-1}$; the concentration of fibrin polymer is shown. The results correspond to simulations for healthy blue mice (A) and following the injection of COVID-19 patient autoantibodies (B). These simulations were conducted using the model described in Section 2.2, which describes the interplay between thrombus growth and blood flow. We consider that the clot is formed in places where the fibrin polymer concentration exceeds 250 nM.

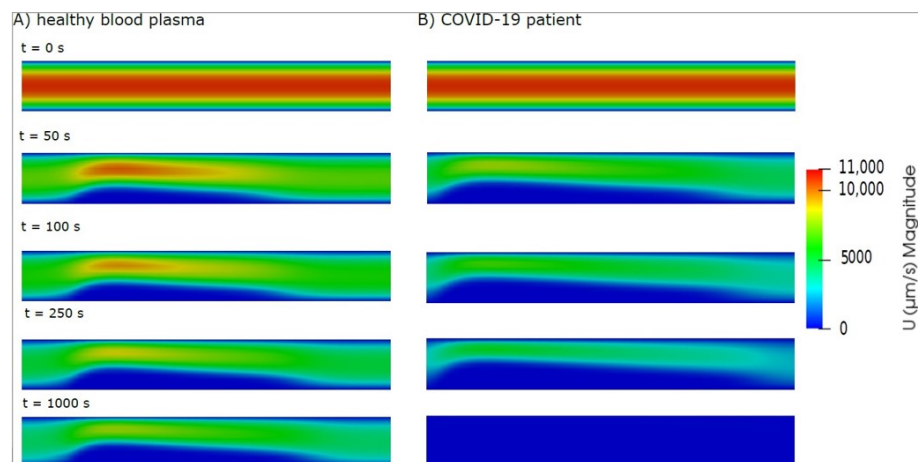


Figure 2. The magnitude of flow velocity during the different stages of clot growth for the healthy mice (A) and after the injection COVID-19 patient autoantibodies (B). We have obtained these results by numerically solving the model described in Section 2.2, using two different parameter sets.

The dynamics of clot growth are presented in Figure 3. These dynamics show that the evolution of the size and height of the clot is almost the same in the healthy subject and the COVID-19 patient during the first 200 s. After this period, the thrombus expands and occludes the vessel rapidly in the COVID-19 patient. The length and size of the clot slightly increase 800 s after the simulation start. The results of these numerical simulations are in a good agreement with the experimental findings [7]. These experiments show that the injection of COVID-19 autoantibodies in mice results in the development of occlusive thrombi in mice. In these experiments, the average length of thrombi in control mice and in mice injected with COVID-19 autoantibodies were 4 mm and 8 mm, respectively. The same values for thrombi length were observed in the numerical simulations.

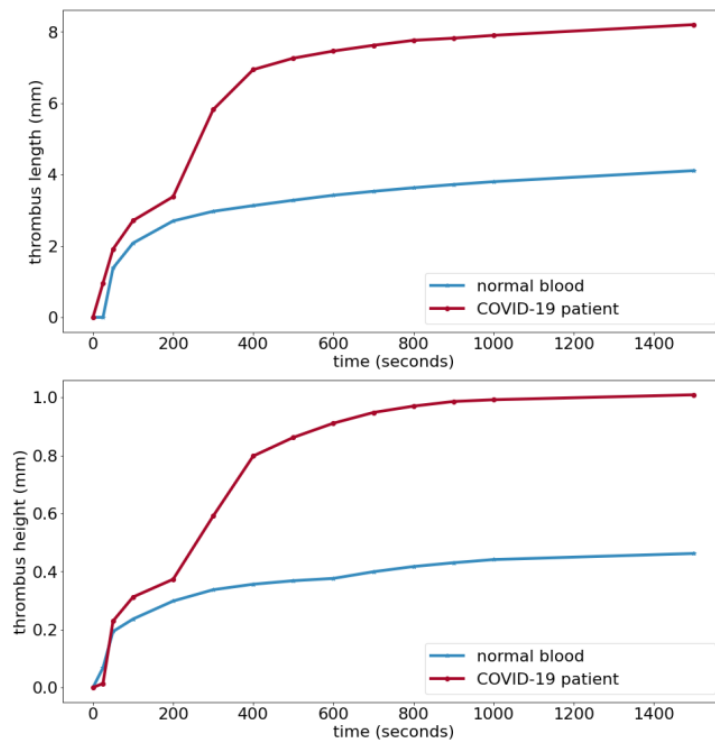


Figure 3. Dynamics of clot growth in the normal bloodstream and after injecting autoantibodies isolated from COVID-19 patients. The length (top) and height (bottom) of the two thrombi are shown over time.

3.2. COVID-19 Autoantibodies Upregulate the Peak Concentration of Thrombin Generation and the Endogenous Thrombin Potential

The calibration of the model allows us to quantify the effect of COVID-19 autoantibodies on the kinetics of the coagulation cascade. In this section, we evaluate the influence of these autoantibodies on thrombin generation curves. These curves can be characterized by four parameters: the lag time, the time to peak, the peak concentration, and the endogenous thrombin potential (ETP) [37]. These parameters are sufficient to characterize any thrombin generation curve. We evaluate the effect of COVID-19 autoantibodies on thrombin generation by studying the effect of the parameter k_3 on the TG curve of a healthy subject. Figure 4A shows that COVID-19 autoantibodies increase the peak concentration and reduce the time needed to reach it. Figure 4B shows a negative linear relationship between the parameter k_3 and time to peak, whereas an exponential relationship can be established between k_3 and the peak concentration (Figure 4C). Finally, a logarithmic relationship is observed between k_3 and the endogenous thrombin potential, as shown in Figure 4D. These predictions qualitatively agree with a clinical study on the effect of COVID-19 on the kinetics of thrombin generation [38].

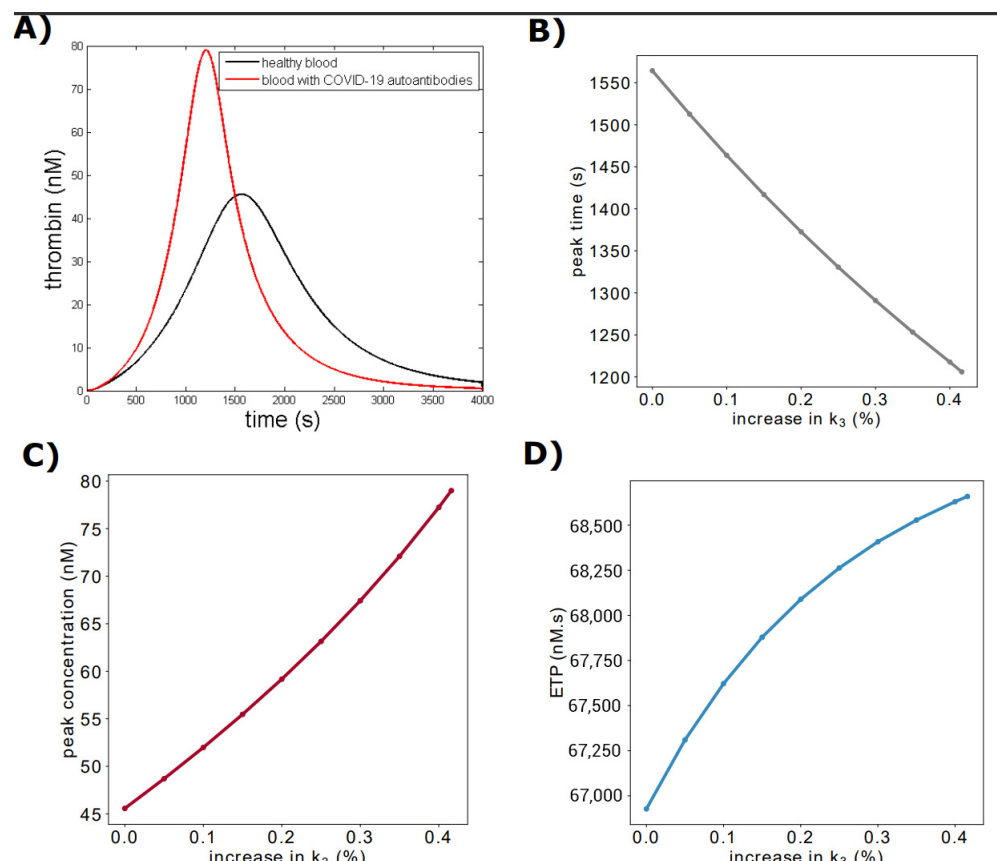


Figure 4. Effect of COVID-19 autoantibodies on the thrombin generation dynamics of a healthy blood plasma. (A) Thrombin generation curves of a healthy subject and a COVID-19 patient. (B) Effect of elevation in k_3 on the time to peak. (C) The peak concentration as a function of k_3 . (D) The endogenous thrombin potential as a function of k_3 .

3.3. Machine Learning Algorithm Predicts the Risk of Thrombosis in COVID-19 Patient

We predict the response of the 3000 virtual patients by solving the corresponding supervised classification problem using machine learning. We use this dataset to train a support vector machine algorithm (SVM). To achieve this, we shuffle the database and divide it into two groups: a training dataset that represents 80% of the data and a test dataset that accounts for the remaining 20%. The algorithm yields an accuracy equal to 94% and can make predictions in a quasi-instantaneous manner. The algorithm was

implemented using the Scikit-learn library in Python v.0.23.2 [39]. In parallel, we train our previously calibrated deep learning algorithm using the same dataset, but we consider four input nodes instead of seven (Figure 5) [29]. The algorithm includes three hidden layers consisting of $500 \times 250 \times 50$ nodes. Initial values of weights were set with the uniform (Xavier) initialization [40]. The Adam learning rate optimization algorithm was used to fit the weights of the ANN [41]; L-2 regularization was used to prevent overfitting. This method consists of adding one more additional term to the loss function. The ReLu activation function was used for all artificial neurons. The trained algorithm predicts the risk of thrombo-embolism with an accuracy of 95%, which is slightly higher than the SVM algorithm. We have previously explored the performance of other architectures and the effects of variations in hyper-parameters on the accuracy of deep learning algorithm [29].

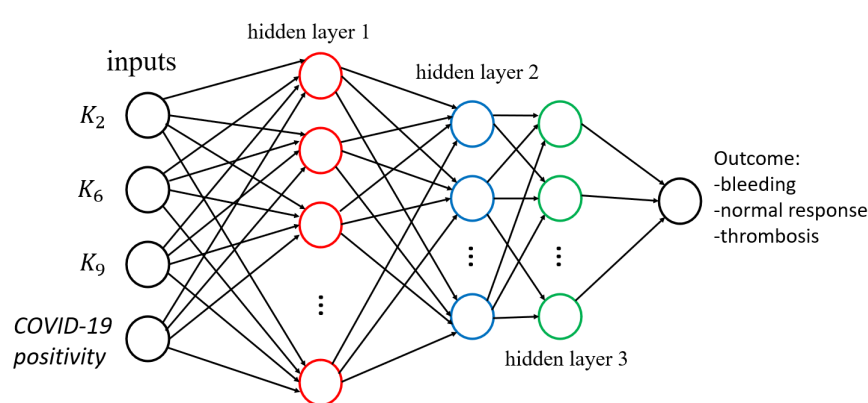


Figure 5. Architecture of the neural network trained to identify the risk of thrombo-embolic events in COVID-19 patients.

4. Discussion

This work presents a novel methodology that aims to evaluate the risk of thrombosis in COVID-19 patients. By detecting the patients with a high risk of developing thromboembolic complications, the algorithm can assist medical doctors in preventing the incidence of cardiovascular events in COVID-19 patients using anticoagulant therapy. The methodology presented in this work harnesses the strengths of both mathematical modelling and machine learning to perform timely and accurate predictions. We used a previously developed model of blood coagulation to study the effect of COVID-19 autoantibodies on clot growth dynamics. The model confirms the hypothesis that was presented in an experimental study [7], which indicates that COVID-19 autoantibodies can cause occlusive venous thrombosis by inducing a hypercoagulable state. By fitting the simulation results to experimental findings of *in vivo* thrombus growth, we were able to quantify the impact of COVID-19 on the kinetics of the coagulation cascade. This quantification enabled us to fit some of the model parameters. As a result, we studied the influence of COVID-19 autoantibodies on thrombin generation. Numerical simulations demonstrate that these autoantibodies reduce the peak time and elevate the peak concentration and endogenous thrombin potential.

The model was simplified and used to generate a large dataset for the hemostatic responses of a cohort of virtual patients. This dataset was used to train a machine learning algorithm capable of predicting the risk of thrombosis in COVID-19 patients in a timely manner. The use of machine learning has several advantages. First, these algorithms make predictions in a quasi-instantaneous manner suitable for clinical use, where the timing of administering treatment is important. Second, they can be easily deployed as smart applications that assist medical doctors and clinicians. However, machine learning is a purely data-driven method that has a few weaknesses. One of them is the lack of interpretability of the obtained predictions. This limitation can be overcome by adding a layer of computational modelling that can be analyzed numerically and theoretically to understand the dynamics of the studied system. Another weakness of machine learning is

the lack of efficacy in dealing with high dimensional data. In this work, we have shown how computational modelling can be used to characterize the thrombin generation curves of real patients and to reduce the dimensionality of the problem.

It is important to note that the objective of this study is to present this new methodology. We do not promote in any way its immediate use in clinical settings. The adoption of this technology in healthcare settings would require more validation efforts against experimental data. To improve the accuracy of the machine learning model, it is possible to replace the considered neural network architecture with more advanced architectures such as the recurrent and convolutional neural networks. Moreover, it would be better to use the 2D version of the model to generate data, but doing so would require access to high-performance computing facilities. Further, we have used experimental data obtained using a thrombosis mouse model to validate the model, but there are a few differences between blood coagulation in humans and in mice. Thus, it would be useful to calibrate the model using data quantifying COVID-19 impact on human thrombus formation in the future. Finally, we have only considered one mechanism of thrombosis pathogenesis in COVID-19 because of the availability of data. Introducing other mechanisms would require access to more quantitative data on their influence on the blood clotting process. COVID-19 influences blood coagulation by other mechanisms, such as the inflammation of endothelial tissue due to the SARS-CoV-2 cytokine storm, which may induce endothelial dysfunction and atherosclerosis. In addition, it was reported that coronavirus infections promotes the activation of fibrinolysis, suggesting a confounding effect of this virus [42].

The presented approach illustrates the advantages of combining mathematical modelling with deep learning to enable the fast and explainable prediction of the coagulation response of specific patients. On one hand, deep learning significantly cut down the CPU time of numerical simulations and can be readily deployed as a smart app that can be used by clinicians. On the other hand, mathematical modelling reduces the dimensionality of the problem and provides explanations for the recommendations made by the machine learning algorithm. These explanations can be obtained by exploring the response of the patients when parameters are perturbed. In this work, we have applied this technique to identify the COVID-19 patients that have an elevated risk of prothrombotic events due to the effect of COVID-19 autoantibodies. The same approach can be used in a variety of applications originating from precision medicine.

Author Contributions: Conceptualization, A.B., P.N. and V.V.; methodology, A.M., V.V. and J.-P.L.; software, A.B.; validation, P.N., J.-P.L. and V.V.; formal analysis, A.B. and A.M.; investigation, P.N. and V.V.; resources, A.B. and V.V.; data curation, A.B. and A.M.; writing—original draft preparation, A.B. and A.M.; writing—review and editing, P.N., J.-P.L. and V.V.; visualization, A.B. and A.M.; supervision, P.N. and V.V.; project administration, V.V.; funding acquisition, A.B. and V.V. All authors have read and agreed to the published version of the manuscript.

Funding: The last author was supported by the RUDN University Scientific Projects Grant System, project No 025141-2-174.

Data Availability Statement: Data are publicly available in the folder “COVID-19” of the following repository: https://github.com/MPS7/ML_coag (accessed on 14 October 2020).

Conflicts of Interest: The authors declare no conflict of interest.

References

1. Levi, M.; Hunt, B.J. Thrombosis and coagulopathy in COVID-19: An illustrated review. *Res. Pract. Thromb. Haemost.* **2020**, *4*, 744–751. [CrossRef]
2. Cui, S.; Chen, S.; Li, X.; Liu, S.; Wang, F. Prevalence of venous thromboembolism in patients with severe novel coronavirus pneumonia. *J. Thromb. Haemost.* **2020**, *18*, 1421–1424. [CrossRef]
3. Iba, T.; Levy, J.H.; Levi, M.; Connors, J.M.; Thachil, J. Coagulopathy of coronavirus disease 2019. *Crit. Care Med.* **2020**, *48*, 1358–1364. [CrossRef]
4. Varga, Z.; Flammer, A.J.; Steiger, P.; Haberecker, M.; Andermatt, R.; Zinkernagel, A.S.; Mehra, M.R.; Schuepbach, R.A.; Ruschitzka, F.; Moch, H. Endothelial cell infection and endotheliitis in COVID-19. *Lancet* **2020**, *395*, 1417–1418. [CrossRef]

5. McGuire, W.W.; Spragg, R.G.; Cohen, A.B.; Cochrane, C.G. Studies on the pathogenesis of the adult respiratory distress syndrome. *J. Clin. Investig.* **1982**, *69*, 543–553. [[CrossRef](#)]
6. Althaus, K.; Marini, I.; Zlamal, J.; Pelzl, L.; Singh, A.; Häberle, H.; Mehrländer, M.; Hammer, S.; Schulze, H.; Bitzer, M.; et al. Antibody-induced procoagulant platelets in severe COVID-19 infection. *Blood* **2021**, *137*, 1061–1071. [[CrossRef](#)]
7. Zuo, Y.; Estes, S.K.; Ali, R.A.; Gandhi, A.A.; Yalavarthi, S.; Shi, H.; Sule, G.; Gockman, K.; Madison, J.A.; Zuo, M.; et al. Prothrombotic autoantibodies in serum from patients hospitalized with COVID-19. *Sci. Transl. Med.* **2020**, *12*, eabd3876. [[CrossRef](#)]
8. Leppkes, M.; Knopf, J.; Naschberger, E.; Lindemann, A.; Singh, J.; Herrmann, I.; Stürzl, M.; Staats, L.; Mahajan, A.; Schauer, C.; et al. Vascular occlusion by neutrophil extracellular traps in COVID-19. *EBioMedicine* **2020**, *58*, 102925. [[CrossRef](#)]
9. Dunster, J.; King, J. Mathematical modelling of thrombin generation: Asymptotic analysis and pathway characterization. *IMA J. Appl. Math.* **2017**, *82*, 60–96. [[CrossRef](#)]
10. Ratto, N.; Tokarev, A.; Chelle, P.; Tardy-Poncet, B.; Volpert, V. Clustering of thrombin generation test data using a reduced mathematical model of blood coagulation. *Acta Biotheor.* **2020**, *68*, 21–43. [[CrossRef](#)]
11. Bouchnita, A.; Terekhov, K.; Nony, P.; Vassilevski, Y.; Volpert, V. A mathematical model to quantify the effects of platelet count, shear rate, and injury size on the initiation of blood coagulation under venous flow conditions. *PLoS ONE* **2020**, *15*, e0235392. [[CrossRef](#)]
12. Bouchnita, A.; Galochkina, T.; Kurbatova, P.; Nony, P.; Volpert, V. Conditions of microvessel occlusion for blood coagulation in flow. *Int. J. Numer. Methods Biomed. Eng.* **2017**, *33*, e2850. [[CrossRef](#)]
13. Zheng, X.; Yazdani, A.; Li, H.; Humphrey, J.D.; Karniadakis, G.E. A three-dimensional phase-field model for multiscale modeling of thrombus biomechanics in blood vessels. *PLoS Comput. Biol.* **2020**, *16*, e1007709. [[CrossRef](#)]
14. Govindarajan, V.; Rakesh, V.; Reifman, J.; Mitrophanov, A.Y. Computational study of thrombus formation and clotting factor effects under venous flow conditions. *Biophys. J.* **2016**, *110*, 1869–1885. [[CrossRef](#)]
15. Leiderman, K.; Fogelson, A.L. Grow with the flow: A spatial–temporal model of platelet deposition and blood coagulation under flow. *Math. Med. Biol. J. IMA* **2011**, *28*, 47–84. [[CrossRef](#)]
16. Bodnár, T.; Sequeira, A. Numerical simulation of the coagulation dynamics of blood. *Comput. Math. Methods Med.* **2008**, *9*, 83–104. [[CrossRef](#)]
17. Wu, W.T.; Jamiolkowski, M.A.; Wagner, W.R.; Aubry, N.; Massoudi, M.; Antaki, J.F. Multi-constituent simulation of thrombus deposition. *Sci. Rep.* **2017**, *7*, 42720. [[CrossRef](#)]
18. Bouchnita, A.; Belyaev, A.V.; Volpert, V. Multiphase continuum modeling of thrombosis in aneurysms and recirculation zones. *Phys. Fluids* **2021**, *33*, 093314. [[CrossRef](#)]
19. Xu, S.; Xu, Z.; Kim, O.V.; Litvinov, R.I.; Weisel, J.W.; Alber, M. Model predictions of deformation, embolization and permeability of partially obstructive blood clots under variable shear flow. *J. R. Soc. Interface* **2017**, *14*, 20170441. [[CrossRef](#)]
20. Tosenberger, A.; Ataullakhanov, F.; Bessonov, N.; Pantelev, M.; Tokarev, A.; Volpert, V. Modelling of thrombus growth in flow with a DPD-PDE method. *J. Theor. Biol.* **2013**, *337*, 30–41. [[CrossRef](#)]
21. Fogelson, A.L.; Guy, R.D. Immersed-boundary-type models of intravascular platelet aggregation. *Comput. Methods Appl. Mech. Eng.* **2008**, *197*, 2087–2104. [[CrossRef](#)]
22. Yazdani, A.; Deng, Y.; Li, H.; Javadi, E.; Li, Z.; Jamali, S.; Lin, C.; Humphrey, J.D.; Mantzoros, C.S.; Em Karniadakis, G. Integrating blood cell mechanics, platelet adhesive dynamics and coagulation cascade for modelling thrombus formation in normal and diabetic blood. *J. R. Soc. Interface* **2021**, *18*, 20200834. [[CrossRef](#)]
23. Xu, Z.; Chen, N.; Kamocka, M.M.; Rosen, E.D.; Alber, M. A multiscale model of thrombus development. *J. R. Soc. Interface* **2008**, *5*, 705–722. [[CrossRef](#)]
24. Li, H.; Deng, Y.; Li, Z.; Dorken Gallastegi, A.; Mantzoros, C.S.; Frydman, G.H.; Karniadakis, G.E. Multiphysics and multiscale modeling of microthrombosis in COVID-19. *PLoS Comput. Biol.* **2022**, *18*, e1009892. [[CrossRef](#)] [[PubMed](#)]
25. Zhu, G.; Modempalli, S.; Anand, M.; Li, H. Computational modeling of hypercoagulability in COVID-19. *Comput. Methods Biomech. Biomed. Eng.* **2022**, 1–12. [[CrossRef](#)] [[PubMed](#)]
26. Mozokhina, A.; Bouchnita, A.; Volpert, V. Blood Clotting Decreases Pulmonary Circulation during the Coronavirus Disease. *Mathematics* **2021**, *9*, 2401. [[CrossRef](#)]
27. Yoon, J.G.; Heo, J.; Kim, M.; Park, Y.J.; Choi, M.H.; Song, J.; Wyi, K.; Kim, H.; Duchenne, O.; Eom, S.; et al. Machine learning-based diagnosis for disseminated intravascular coagulation (DIC): Development, external validation, and comparison to scoring systems. *PLoS ONE* **2018**, *13*, e0195861. [[CrossRef](#)]
28. Fang, K.; Dong, Z.; Chen, X.; Zhu, J.; Zhang, B.; You, J.; Xiao, Y.; Xia, W. Using machine learning to identify clotted specimens in coagulation testing. *Clin. Chem. Lab. Med. (CCLM)* **2021**, *59*, 1289–1297. [[CrossRef](#)] [[PubMed](#)]
29. Bouchnita, A.; Nony, P.; Llored, J.P.; Volpert, V. Combining mathematical modeling and deep learning to make rapid and explainable predictions of the patient-specific response to anticoagulant therapy under venous flow. *Math. Biosci.* **2022**, *349*, 108830. [[CrossRef](#)]
30. Krasotkina, Y.V.; Sinauridze, E.I.; Ataullakhanov, F.I. Spatiotemporal dynamics of fibrin formation and spreading of active thrombin entering non-recalcified plasma by diffusion. *Biochim. Biophys. Acta (BBA)-Gen. Subj.* **2000**, *1474*, 337–345. [[CrossRef](#)]
31. Bessonov, N.; Sequeira, A.; Simakov, S.; Vassilevskii, Y.; Volpert, V. Methods of blood flow modelling. *Math. Model. Nat. Phenom.* **2016**, *11*, 1–25. [[CrossRef](#)]

32. Wufsus, A.R.; Macera, N.; Neeves, K. The hydraulic permeability of blood clots as a function of fibrin and platelet density. *Biophys. J.* **2013**, *104*, 1812–1823. [[CrossRef](#)] [[PubMed](#)]
33. Jasak, H.; Jemcov, A.; Tukovic, Z. OpenFOAM: A C++ library for complex physics simulations. In Proceedings of the International Workshop on Coupled Methods in Numerical Dynamics, Dubrovnik, Croatia, 19–21 September 2007; Volume 1000, pp. 1–20.
34. Xu, Z.; Shi, L.; Wang, Y.; Zhang, J.; Huang, L.; Zhang, C.; Liu, S.; Zhao, P.; Liu, H.; Zhu, L.; et al. Pathological findings of COVID-19 associated with acute respiratory distress syndrome. *Lancet Respir. Med.* **2020**, *8*, 420–422. [[CrossRef](#)] [[PubMed](#)]
35. Wang, Y.; Luo, L.; Braun, O.Ö.; Westman, J.; Madhi, R.; Herwald, H.; Mörgelin, M.; Thorlacius, H. Neutrophil extracellular trap-microparticle complexes enhance thrombin generation via the intrinsic pathway of coagulation in mice. *Sci. Rep.* **2018**, *8*, 4020. [[CrossRef](#)]
36. Galochkina, T.; Bouchnita, A.; Kurbatova, P.; Volpert, V. Reaction-diffusion waves of blood coagulation. *Math. Biosci.* **2017**, *288*, 130–139. [[CrossRef](#)]
37. Hemker, H.C.; Béguin, S. Thrombin generation in plasma: Its assessment via the endogenous thrombin potential. *Thromb. Haemost.* **1995**, *74*, 134–138. [[CrossRef](#)]
38. De la Morena-Barrio, M.E.; Bravo-Pérez, C.; Miñano, A.; de la Morena-Barrio, B.; Fernandez-Perez, M.P.; Bernal, E.; Gómez-Verdu, J.M.; Herranz, M.T.; Vicente, V.; Corral, J.; et al. Prognostic value of thrombin generation parameters in hospitalized COVID-19 patients. *Sci. Rep.* **2021**, *11*, 7792. [[CrossRef](#)]
39. Pedregosa, F.; Varoquaux, G.; Gramfort, A.; Michel, V.; Thirion, B.; Grisel, O.; Blondel, M.; Prettenhofer, P.; Weiss, R.; Dubourg, V.; et al. Scikit-learn: Machine learning in Python. *J. Mach. Learn. Res.* **2011**, *12*, 2825–2830.
40. Glorot, X.; Bengio, Y. Understanding the difficulty of training deep feedforward neural networks. In Proceedings of the Thirteenth International Conference on Artificial Intelligence and Statistics, JMLR Workshop and Conference Proceedings, Sardinia, Italy, 13–15 May 2010; pp. 249–256.
41. Kinga, D.P. A method for stochastic optimization. In Proceedings of the International Conference on Learning Representations (ICLR), San Deigo, CA, USA, 7–9 May 2015.
42. Levi, M.; Thachil, J.; Iba, T.; Levy, J.H. Coagulation abnormalities and thrombosis in patients with COVID-19. *Lancet Haematol.* **2020**, *7*, e438–e440. [[CrossRef](#)]

Disclaimer/Publisher’s Note: The statements, opinions and data contained in all publications are solely those of the individual author(s) and contributor(s) and not of MDPI and/or the editor(s). MDPI and/or the editor(s) disclaim responsibility for any injury to people or property resulting from any ideas, methods, instructions or products referred to in the content.